AIP Journal of Applied Physics

Enhancing electrical conductivity and electron field emission properties of ultrananocrystalline diamond films by copper ion implantation and annealing

K. J. Sankaran, K. Panda, B. Sundaravel, N. H. Tai, and I. N. Lin

Citation: Journal of Applied Physics **115**, 063701 (2014); doi: 10.1063/1.4865325
View online: http://dx.doi.org/10.1063/1.4865325
View Table of Contents: http://scitation.aip.org/content/aip/journal/jap/115/6?ver=pdfcov
Published by the AIP Publishing

Articles you may be interested in

Direct observation and mechanism for enhanced field emission sites in platinum ion implanted/post-annealed ultrananocrystalline diamond films
Appl. Phys. Lett. **105**, 163109 (2014); 10.1063/1.4898571

Gold ion implantation induced high conductivity and enhanced electron field emission properties in ultrananocrystalline diamond films
Appl. Phys. Lett. **102**, 061604 (2013); 10.1063/1.4792744

Direct observation of enhanced emission sites in nitrogen implanted hybrid structured ultrananocrystalline diamond films
J. Appl. Phys. **113**, 054311 (2013); 10.1063/1.4790481

Structural and electronic properties of nitrogen ion implanted ultra nanocrystalline diamond surfaces
J. Appl. Phys. **110**, 044304 (2011); 10.1063/1.3622517

n-type conductivity and phase transition in ultrananocrystalline diamond films by oxygen ion implantation and annealing
J. Appl. Phys. **109**, 053524 (2011); 10.1063/1.3556741

[This article is copyrighted as indicated in the article. Reuse of AIP content is subject to the terms at: http://scitation.aip.org/termsconditions. Downloaded to] IP: 163.13.36.187 On: Mon, 27 Oct 2014 02:56:23

JOURNAL OF APPLIED PHYSICS 115, 063701 (2014)

Enhancing electrical conductivity and electron field emission properties of ultrananocrystalline diamond films by copper ion implantation and annealing

K. J. Sankaran,[1] K. Panda,[2] B. Sundaravel,[2] N. H. Tai,[1,a)] and I. N. Lin[3,a)]
[1]*Department of Materials Science and Engineering, National Tsing-Hua University, Hsinchu 300, Taiwan*
[2]*Materials Science Group, Indira Gandhi Centre for Atomic Research, Kalpakkam 603 102, India*
[3]*Department of Physics, Tamkang University, Tamsui 251, Taiwan*

(Received 23 January 2014; accepted 28 January 2014; published online 10 February 2014)

Copper ion implantation and subsequent annealing at 600 °C achieved high electrical conductivity of 95.0 $(\Omega\text{cm})^{-1}$ for ultrananocrystalline diamond (UNCD) films with carrier concentration of $2.8 \times 10^{18}\,\text{cm}^{-2}$ and mobility of $6.8 \times 10^{2}\ \text{cm}^2/\text{V s}$. Transmission electron microscopy examinations reveal that the implanted Cu ions first formed Cu nanoclusters in UNCD films, which induced the formation of nanographitic grain boundary phases during annealing process. From current imaging tunneling spectroscopy and local current-voltage curves of scanning tunneling spectroscopic measurements, it is observed that the electrons are dominantly emitted from the grain boundaries. Consequently, the nanographitic phases presence in the grain boundaries formed conduction channels for efficient electron transport, ensuing in excellent electron field emission (EFE) properties for copper ion implanted/annealed UNCD films with low turn-on field of 4.80 V/μm and high EFE current density of 3.60 mA/cm^2 at an applied field of 8.0 V/μm. © *2014 AIP Publishing LLC*. [http://dx.doi.org/10.1063/1.4865325]

I. INTRODUCTION

Cold cathode materials with outstanding electron field emission (EFE) characteristics, such as low turn-on field and high current density, have been very useful for vacuum electronic devices such as electron source for high energy accelerators, electron microscopes, X-ray sources, cathode-ray tube monitors, and microwave amplifiers.[1–3] Diamond is a good electronic candidate for solid-state electronics emitters because of its negative electron affinity (NEA) surface.[4–6] Ultrananocrystalline diamond (UNCD) film, which acquires ultrasmall grain sizes of 5–10 nm with very smooth film surfaces, has recently attained broad interest because of its superb EFE behavior as compared to that of microcrystalline and nanocrystalline diamond films.[7,8] The grains in UNCD films consist of sp^3 character and the grain boundaries contain a mixture of sp^2, sp^3, hydrocarbon and amorphous carbon (*a-C*), in which the sp^2 phases are the predominant phases.[9] Inducing graphitic grain boundary phases by incorporation of N_2 into plasma during UNCD film's growth can efficiently improve the electrical conductivity and the EFE properties of the films.[10–13] However, high growth temperature (about 800 °C) is entailed to activate the dopants for creating the admirable conductivity in the UNCD films.[14,15]

Alternatively, ion implantation has been suggested as a possible way to incorporate a variety of dopants for creating highly conducting UNCD films.[16–21] Oxygen and phosphorous ion implantation on UNCD films provide *n*-type conductivity but the electrons are transported through the films by the *a-C* grain boundaries.[20,21] However, the conductivity of *a-C* grain boundary phases of UNCD films is not adequately high and consequently restrains the EFE properties achievable for UNCD films.[8] Converting *a-C* in the grain boundaries of UNCD films into crystalline carbon seems to be the right track in further enhancing the conductivity of the UNCD films. In contrast, Au ion implantation has been observed to markedly enhance the EFE properties of UNCD films,[19] due to the induction of graphitic phases in the grain boundaries of UNCD films. However, the Au ions are deep donors,[22] which are harmful in the manufacturing of Si-based devices such as integrated circuits and solar cells. The search for ions which are more compatible with the Si-based devices and enhancement of the EFE properties of the UNCD films is necessary. Copper is widely used as interconnects and contact materials in electronics and ultra large scale integration due to its low cost, excellent electrical conductivity (1.67 $\mu\Omega$ cm for bulk) and good electromigration resistance.[23,24] Recently, Cu ion implantation has been observed to locally modify the surface of silica glass to create periodic plasmonic microstructures with Cu nanoparticles,[25] to induce the ferromagnetism in GaN,[26,27] and to provoke the formation of *a-C* and/or graphite like phase in the polycarbonate matrices, rendering them conducting.[28,29] Moreover, Cu has been utilized for synthesizing the graphene in chemical vapor deposition process, implying that Cu has some degree of solubility to carbon species and catalytically induce the formation of sp^2-bonded carbons.[30] Therefore, it sees that Cu ions are appropriate for ion implantation into UNCD films to trigger the formation of nanographite clusters so as to enhance the EFE properties for these films.

In this context, UNCD films were implanted by Cu ions followed by annealing at 600 °C for obtaining high electrical conductivity and superior EFE properties of UNCD films. Importantly, current imaging tunneling microscopy (CITS) in scanning tunneling spectroscopy (STS) mode is used to

a)Electronic addresses: nhtai@mx.nthu.edu.tw and inanlin@mail.tku.edu.tw.

 © 2014 AIP Publishing LLC

[This article is copyrighted as indicated in the article. Reuse of AIP content is subject to the terms at: http://scitation.aip.org/termsconditions. Downloaded to] IP: 163.13.36.187 On: Mon, 27 Oct 2014 02:56:23

directly detect the increased emission site densities in Cu ion implanted/annealed UNCD films than the pristine UNCD films in nanometer scale. The modifications to the microstructure of these films due to Cu ion implantation/annealing processes were investigated in detail using transmission electron microscopy (TEM). We observed that the possible mechanism of high electrical conductivity and improved EFE properties of UNCD films is the induction of nanographite phases in the films.

II. EXPERIMENTAL

UNCD films were grown on *n*-type silicon substrates in a microwave plasma enhanced chemical vapor deposition system (2.45 GHz, 6″ IPLAS-CYRANNUS-I, Troisdorf, Germany). The Si substrates were first thoroughly cleaned by rinsing the Si substrates in a water-diluted hydrogen peroxide/ammonium hydroxide and hydrogen peroxide/hydrochloric acid solution sequentially. Then the cleaned Si substrates were ultrasonicated in methanol solution containing nanodiamond powders (about 4 nm in size) and titanium powders (<32.5 nm) (SIGMA ALDRICH) for 45 min to facilitate the nucleation of diamond. The UNCD films were grown on the Si substrates in a CH_4/Ar = 1/99 sccm plasma excited by 1200 W microwave power with 200 mbar pressure for 3 h to a thickness about 1 μm. No external heater was used to heat the substrate. The substrate was heated up by plasma bombardment to a temperature of 470 °C, which was monitored by a thermocouple embedded in the stainless steel substrate holder. The 300 keV copper ions with an ion fluence of 1×10^{17} ions/cm^2 were implanted on UNCD films at room temperature in a pressure below 2×10^{-7} mbar, followed by annealing at 600 °C in N_2 atmosphere for 30 min. The pristine UNCD films are designated as "UNCD$_P$," whereas the Cu ion implanted/annealed films are called as "UNCD$_{CuA}$."

Hall measurements were carried out in a van der Pauw configuration (ECOPIA HMS-3000) to observe the conducting behavior of these films. The EFE properties of the samples were measured with a parallel plate setup, in which the cathode (UNCD films)-to-anode (molybdenum rod with a diameter of 2 mm) distance was controlled using a micrometer. The current density versus electrical field (*J-E*) characteristics were measured using an electrometer (Keithley 2410) at pressure below 1.3×10^{-6} mbar. The EFE characteristics of materials were molded using the Fowler-Nordheim (F-N) theory.[31] The local electron emission behavior in the ion implanted UNCD films was investigated by ultra high vacuum-scanning tunneling microscopy (UHV STM; 150 Aarhus, SPECS GmbH, Germany). The STM tips were prepared by electrochemical etching of tungsten wires and the measurements were proceeded at room temperature with a base pressure of 10^{-10} mbar. The STM imaging was performed with a constant current of 0.59 nA and a bias voltage of −5 V. CITS with voltages ramping from −5 to 5 V were measured concurrently during the STM image scanning at fixed height of tip over the examined region. A STS spectrum was computed from an average of many I–V curves taken at different positions in the STM image.

The surface morphology of the films was investigated by field emission scanning electron microscopy (FESEM; JEOL-6500). The crystalline quality and the depth profile of the UNCD films was characterized by Raman spectroscopy (Lab Raman HR800, Jobin Yvon; $\lambda = 632$ nm) and secondary ions mass spectroscopy (SIMS; Cameca IMS-4f), respectively. The chemical bonding structures of the films were investigated by X-ray photoelectron spectroscopy (XPS; PHI 1600). High resolution transmission electron microscopy (HRTEM; JEOL-2100 F) was examined to characterize the microstructures of the UNCD films.

III. RESULTS AND DISCUSSION

A. Materials characteristics

The SIMS depth profile shown in Fig. 1 suggests that copper ions are implanted into UNCD films to a depth of about 560 nm with peak concentration located at around 250 nm beneath the surface. This profile confirms that Cu ions have been implanted in the UNCD films. Fig. 2(a) shows Hall measurements of UNCD films in a van der Pauw configuration with the measuring probes directly in contact with the films [inset of Fig. 2(a)]. While the UNCD$_P$ films are too resistive to be measured using the van der Pauw configuration [curve I, Fig. 2(a)], the UNCD$_{CuA}$ films show high electrical conductivity of 95.0 $(\Omega\ \mathrm{cm})^{-1}$ with carrier concentration of 2.8×10^{18} cm^{-2} and mobility of 6.8×10^2 cm^2/V s [curve II, Fig. 2(a)]. The obtained electrical conductivity of UNCD$_{CuA}$ films are higher than that of the phosphorous and oxygen ion implanted UNCD films (see Table I).[20,21]

The effect of Cu ion implantation/annealing processes in modifying the EFE properties of UNCD films is shown in Fig. 2(b) with the inset indicating the corresponding F-N plot. The turn-on field (E_0) is designated as the interception of the high and low-field line segments of the F-N plots, viz., $\ln(J_e/E^2)$ versus $1/E$ [inset of Fig. 2(b)]. The Cu ion implantation/annealing processes improved markedly the EFE properties of the UNCD films that are evidently due to the increase in conductivity of the films. The E_0 value for the EFE process decreased from $(E_0)_{UNCDP} = 17.1$ V/μm for UNCD$_P$ films [curve I, Fig. 2(b)] to $(E_0)_{UNCDCuA} = 4.80$ V/μm for UNCD$_{CuA}$ films, whereas the EFE current density increased

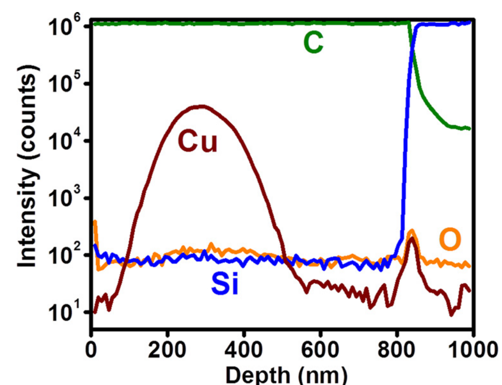

FIG. 1. SIMS depth profiles of C, Cu, Si, and O species in Cu ion implanted/annealed (UNCD$_{CuA}$) films.

[This article is copyrighted as indicated in the article. Reuse of AIP content is subject to the terms at: http://scitation.aip.org/termsconditions. Downloaded to] IP: 163.13.36.187 On: Mon, 27 Oct 2014 02:56:23

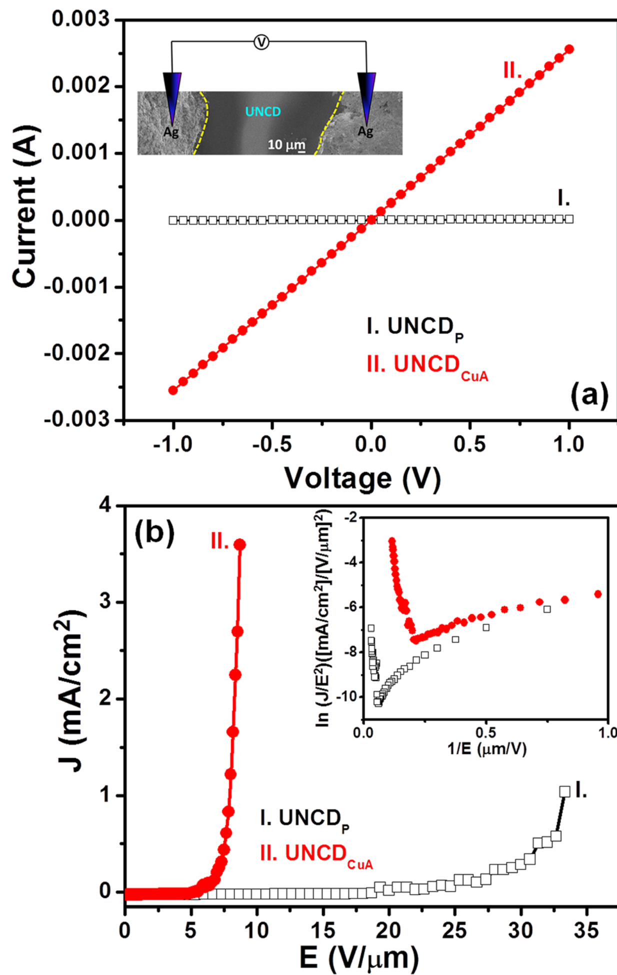

FIG. 2. (a) Electrical conductivity and (b) electron field emission properties of I. UNCD$_P$, II. UNCD$_{CuA}$ films. The inset of (b) shows the corresponding Fowler-Nordheim (F-N) plot.

from $(J)_{UNCDP} = 1.03\,mA/cm^2$ (at an applied field of 33.5 V/μm) to $(J)_{UNCDCuA} = 3.60\,mA/cm^2$ (at an applied field of 8.0 V/μm). Such kind of EFE properties of UNCD$_{CuA}$ films are comparable to that of conducting UNCD films ever reported (see Table I).[13,19]

Fig. 3(a) shows the morphological changes in the UNCD films due to Cu ion implantation/annealing processes using field emission scanning electron microscopy (FESEM; JEOL-6500). The UNCD$_P$ films contain equi-axed ultrasmall grain microstructure. The Cu ions implantation/annealing processes rendered the surface morphology of UNCD$_P$ films to a featureless surface morphology [inset of Fig. 3(a)]. The effect of Cu ion implantation/annealing processes on altering the bonding characteristics of UNCD films is investigated using visible-Raman spectroscopy. The Raman spectra were deconvoluted by using the multi-peak Lorentzian fitting method and are shown in Fig. 3(b). Peaks at around 1160 cm^{-1} and 1475 cm^{-1} are attributed to the ν_1 and ν_3 modes of *trans*-polyacetylene (*t*-PA) present in the grain boundaries of UNCD$_P$ films [curve I, Fig. 3(b)].[32,33] A broadened peak around 1340 cm^{-1} (designated as D*-band), which corresponds to the disordered sp^2 bonded carbon, is observed in UNCD$_P$ films.[34,35] The G-band of the UNCD$_P$ films is observed at around 1540 cm^{-1}. A shoulder peak around 1600 cm^{-1} (designated as G′ band) is seen that possibly arises from the nanocrystalline graphitic content in the films.[35] Raman resonance D peak at 1332 cm^{-1} corresponding to sp^3-bonded carbon shows less intensity for UNCD$_P$ films, because the visible-Raman spectroscopy is more sensitive to sp^2-bonded carbon as compared to that of sp^3-bonded one.[7] The Cu ion implantation/annealing processes altered the bonding characteristics of the UNCD films markedly that is shown in curve II of Fig. 3(b). This figure shows higher intensities of D* and G peaks and the higher intensity of G′ band is also observed for UNCD$_{CuA}$ films. These observations indicate

TABLE I. Comparison on the electrical conductivity measured and turn-on field of electron field emission for the conducting UNCD films.

Materials	Electrical conductivity $(\Omega\,cm)^{-1}$	Turn-on field (V/μm)	References
N_2 doped UNCD	200	6.13	13
Au ion implanted UNCD	185	4.88	19
O_2 ion implanted UNCD/annealing	33.3	–	20
P ion implanted UNCD/annealing	0.09	–	21
Cu ion implanted UNCD/annealing	95	4.80	This study

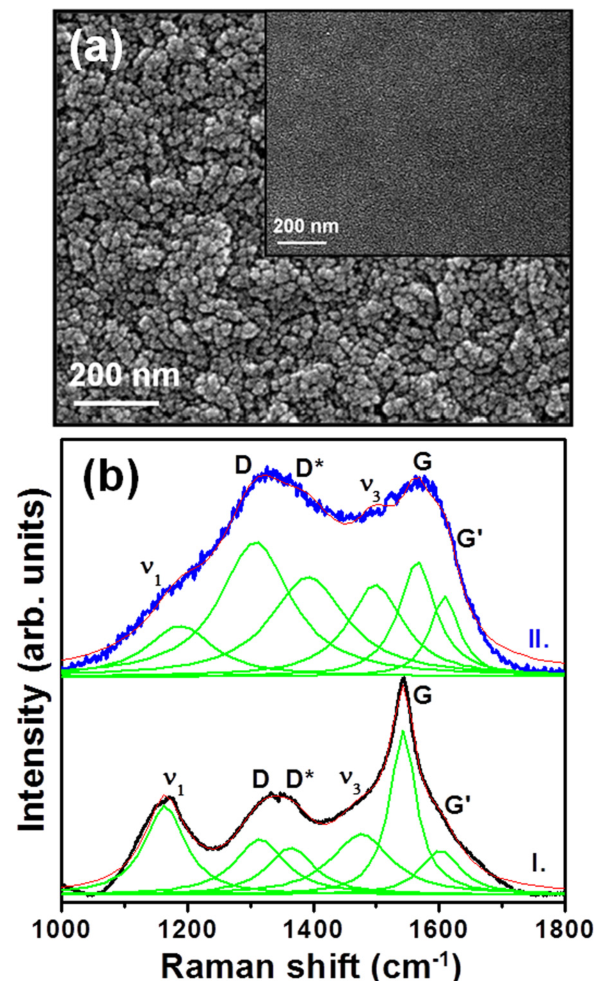

FIG. 3. (a) FESEM image of UNCD$_P$ films with inset shows the FESEM image of UNCD$_{CuA}$ films. (b) visible-Raman spectra of I. UNCD$_P$ and II. UNCD$_{CuA}$ films taken with 632 nm laser line.

[This article is copyrighted as indicated in the article. Reuse of AIP content is subject to the terms at: http://scitation.aip.org/termsconditions. Downloaded to] IP: 163.13.36.187 On: Mon, 27 Oct 2014 02:56:23

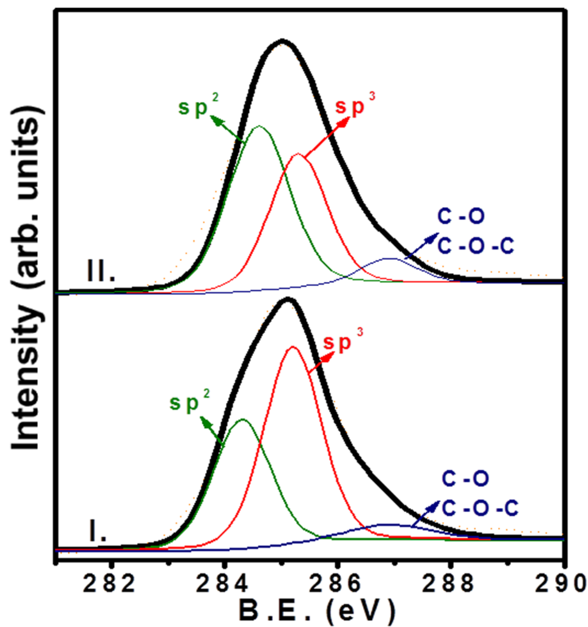

FIG. 4. C1s XPS spectra of I. $UNCD_P$ and II. $UNCD_{CuA}$ films.

amorphization and graphitization type of transitions in the UNCD films due to Cu ion implantation and annealing. The position of the ν_1 and ν_3 bands shifted to higher wave numbers. The shifting is probably a sign of the breaking of *t*-PA chains due to Cu ion implantation/annealing processes. The increase of the I_D/I_G values and G band shift to higher wave number imply the formation of nanographite phases and decrease in sp^3 content according to increasing disorder in carbon materials.[35,36] That is, there is conversion of sp^3 to sp^2 content. Restated the disorder/*a-C* phases are converted into graphitic phases due to the Cu ion implantation/annealing processes of UNCD films.

The surface chemical bonding characteristics of UNCD films were investigated by X-ray photoelectron microscopy (XPS; PHI 1600). The C1s photoemission spectra of UNCD films are shown in Fig. 4. The measurement was conducted without ion sputtering etching to avoid reconfiguration of the bonds. The background was subtracted using Shirley's method[37] and the data were fitted with Lorentzian peaks with binding energies at 284.4, 285.1, and 287.0 eV corresponding to sp^2 C=C, sp^3 C-C and C-O/C-O-C bonds, respectively. Their relative intensities are tabulated in Table II. In $UNCD_P$ films [curve I, Fig. 4], sp^3 C-C bonding is predominant with the peak intensity of 55.3% accompanying with sp^2 C=C intensity of 36.7% and C-O/C-O-C peak intensity of 8.0%; whereas, in $UNCD_{CuA}$ films, sp^2 C=C peak is predominant with the peak intensity of 71.5% [curve II of Fig. 4]. The increase in sp^2 content upon Cu ion implantation/annealing is consistent with our Raman data [c.f. Fig. 3(b)]. Conspicuously, we have found the significant $Cu2p_{3/2}$ and $Cu2p_{1/2}$ peaks from $UNCD_{CuA}$ films (figure not shown), implying that Cu ions aggregated to form Cu nanoclusters due to Cu ion implantation.

TABLE II. Relative intensities of various components of C1s XPS spectra for pristine ($UNCD_P$) and Cu ion implanted/annealed ($UNCD_{CuA}$) UNCD films.

	Chemical bonding (%)		
Samples	sp^2 C=C (284.2)	sp^3 C-C (285.1)	CO/C-O-C (287.0)
$UNCD_P$	36.7	55.3	8.0
$UNCD_{CuA}$	71.5	25.2	3.3

B. Scanning tunneling spectroscopy

To reveal how the changes in microstructure and concentrations of sp^2 and sp^3 phases affect the EFE properties of these films, the local electronic properties of the films were investigated by CITS in STS mode to directly divulge the emission sites in these films. STS measurements of pristine and Cu ion implanted/annealed UNCD films were systematically performed to study the effect of these processes on the density of emission sites. Pristine UNCD films are resistive for STM measurements. The surface of $UNCD_P$ film became conducting when sputter ion-etched with Ar^+ ions for 1 min by removing nearly 1 nm thickness inside the XPS chamber. STM measurements are made after that and Fig. 5(a) shows the STM image of $UNCD_P$ film surface. The grain size of

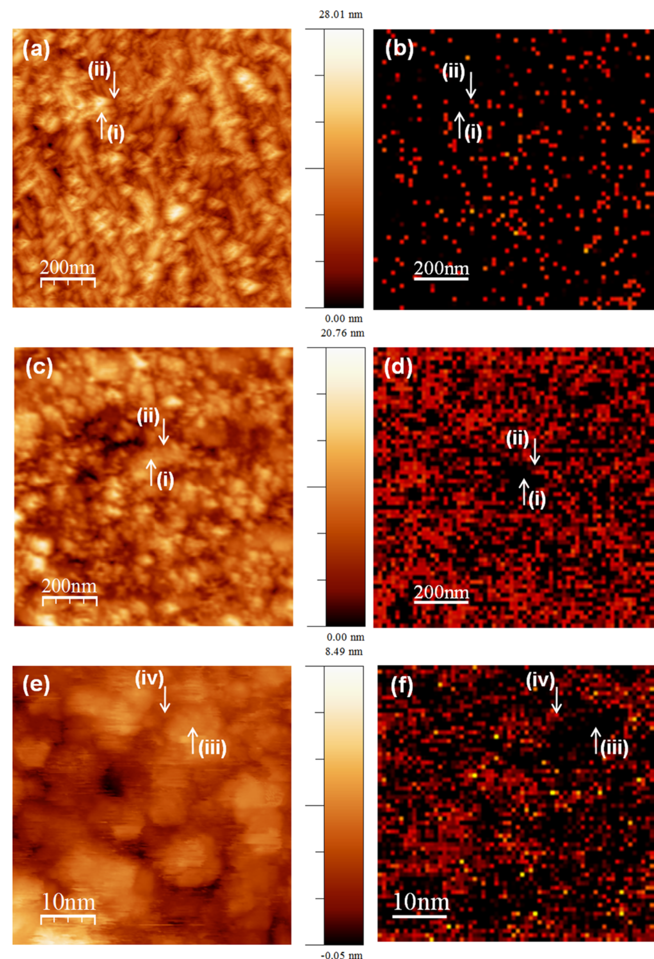

FIG. 5. The STM image of (a) $UNCD_P$ and (c) $UNCD_{CuA}$ films with (b) and (d) showing the CITS image corresponding to (a) and (c); the HRSTM image of (e) $UNCD_{CuA}$ UNCD films with (f) the corresponding CITS image. The CITS images were acquired at a sample bias of −5 V.

[This article is copyrighted as indicated in the article. Reuse of AIP content is subject to the terms at: http://scitation.aip.org/termsconditions. Downloaded to] IP: 163.13.36.187 On: Mon, 27 Oct 2014 02:56:23

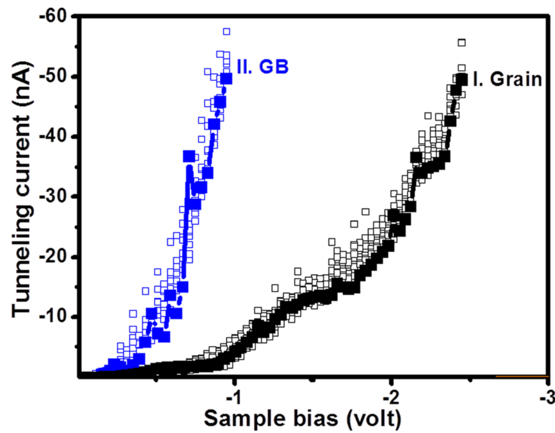

FIG. 6. The (a) local I-V curves obtained in STS measurements at the grain "G" and the grain boundary "GB" of $UNCD_{CuA}$ films [marked as "iii" and "iv" in high resolution STM image in Fig. 5(e)], where the thick line drawn corresponds to the average of 10 I-V curves at the designated points.

$UNCD_P$ film is between 3 and 5 nm, and a grain of 5 nm size, marked as "i," is not very smooth due to sputtering. A typical grain boundary is marked as "ii." Fig. 5(b) shows the current map of CITS image corresponding to Fig. 5(a) taken at a sample bias of −5 V. Bright and dark regions in CITS image are visible with their shapes having similarity with the shapes of grain boundaries (ii) and grains (i) of the STM image in Fig. 5(b), respectively. Bright contrast in the CITS image represents better electron emission.[31] The CITS image (Fig. 5(b)) shows clearly that the emission sites are mainly located along the grain boundaries.

Figure 5(c) shows that there are presence of ultra-smaller grains which occur due to the Cu ion implantation/annealing processes and the corresponding CITS image is shown in Fig. 5(d), taken at a sample bias of −5 V. Typical grains and grain boundaries in this image are marked as "i" and "ii," respectively. The corresponding positions in the CITS image (Fig. 5(d)) are also marked "i" and "ii". Interestingly, the emission site density increases significantly in $UNCD_{CuA}$ films than $UNCD_P$ films. It looks as if the whole film surface emits. Figure 5(e) shows the high resolution STM (HRSTM) image of $UNCD_{CuA}$ films. We could observe uniform diamond grains of nearly 5 nm. Typical grain and grain boundary are marked as "iii" and "iv" in Fig. 5(e). Figure 5(f) shows the CITS image corresponding to Fig. 5(e) taken at the sample bias of −5 V. It is observed that the emission sites are along the grain boundaries of the smaller grains marked as "iv" in Fig. 5(f), indicating that grain boundaries are the prominent electron emission sites.

The local electronic properties are characterized by measuring the local current versus voltage (I-V) curves of $UNCD_{CuA}$ films from STS measurements at various sample positions as on the grains and grain boundaries in HRSTM image shown in Fig. 5(e). Only the negative portion of the I-V curves is shown in Fig. 6, as the negatively biased current corresponds to the tunneling of electrons from the diamond surface to the tungsten tip and is proportional to the density of occupied states in the diamond. Ten reproducible I-V spectra corresponding to each emission sites (grain and grain boundaries of $UNCD_{CuA}$ film as shown in Fig. 5(e)) were recorded during the I-V measurements. It should be noted that the curves "G" and "GB" correspond to grain and grain boundary of $UNCD_{CuA}$ films, respectively (locations "iii" and "iv" in Fig. 5(e), respectively). We observed a significant change in I-V characteristic curves both at the grain and at the grain boundary for $UNCD_{CuA}$ films. The grain boundaries (curve II) emit at a lower sample bias compared to the grains (curve I). Moreover, the conductivity of the grain boundaries is better than that of grains in both films, which is consistent with the CITS image, showing bright emissions around the grain boundaries shown in Figs. 5(e) and 5(f).

C. Transmission electron microscopy

The STS measurements illustrate clearly the benefit of Cu ion implantation/annealing processes on increasing the number density of field emission sites. However, the authentic factor for such an effect is still not clear. The microstructural evolution induced by the Cu ion implantation/annealing processes is actually more important information for understanding the change in electrical conductivity and EFE properties of $UNCD_{CuA}$ films. The microstructure of the $UNCD_{CuA}$ films was examined using TEM (JEOL-2100 F, 200 eV). Fig. 7(a) shows the typical bright field image for the $UNCD_{CuA}$ films. Inset in Fig. 7(a) shows the selective area electron diffraction (SAED) pattern which illustrates that, besides the diffraction rings corresponding to the $(111)_D$, $(220)_D$, and $(311)_D$ lattice planes of diamond, there presents an extra diffraction ring corresponding to Cu material (designated as $(111)_{Cu}$). To elucidate the localized bonding structure of the UNCD films, the selective area electron energy loss spectra (EELS) of the films were acquired and were shown in Figs. 7(b) and 7(c). Notably, the EELS spectra of $UNCD_P$ films were included in these figures (curve I) to facilitate the comparison. Core-loss EELS spectrum shown as curve II in Fig. 7(b) indicates a small hump, representing sp^2-bonded carbon (285 eV, π^*-band) besides the typical EELS signal of sp^3-bonded carbon, i.e., a sharp peak at 290 eV (σ^*-band) and a dip in the vicinity of 302 eV.[38,39] Moreover, plasmon-loss EELS spectrum shown as curve II of Fig. 7(c) reveals that the sp^2-bonded carbon contained in these films is graphitic in nature, as it contains a large diffuse peak near 27 eV.[40] Particularly, for a plasmon-loss EELS spectrum corresponding to sp^3-bonded carbon in a diamond material, a peak near 33 eV (ω_{d2}-peak) representing the bulk plasma of diamond clusters with a shoulder near 23 eV (ω_{d1}-peak) representing surface plasma of the clusters should be observed which are illustrated in curve I of Fig. 7(c).[40]

Figure 8 shows the structure image for $UNCD_{CuA}$ films corresponding to region A in Fig. 7(a). Fourier transformed (FT) diffractogram of the whole structure image (FT_0) shows a spotted diffraction pattern arranged in ring, suggesting of nano-sized nature of the diamond (D) and the copper (Cu) phases. The diffused diffraction ring located at the center of FT image corresponds to graphitic (G) phase. The existence of diamond (D) and copper (Cu) phases are highlighted by regions 1 and 2, respectively, which are identified by the FT images FT_1 and FT_2, respectively. The presence of graphitic

[This article is copyrighted as indicated in the article. Reuse of AIP content is subject to the terms at: http://scitation.aip.org/termsconditions. Downloaded to] IP: 163.13.36.187 On: Mon, 27 Oct 2014 02:56:23

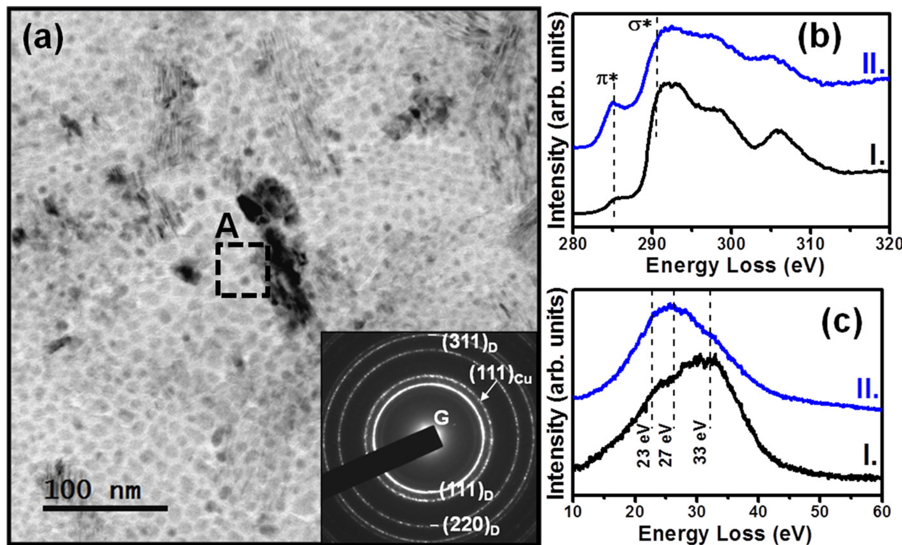

FIG. 7. (a) TEM micrograph of $UNCD_{CuA}$ films with corresponding SAED pattern is shown as inset. (b) Carbon edge core-loss and (c) plasmon-loss EELS spectra of I. $UNCD_P$ films and II. $UNCD_{CuA}$ films.

phases near the Cu nanoclusters was highlighted by region 3 that is confirmed by the FT image FT_3. Notably, the Cu nanoclusters [region 2, Fig. 8] are not sharply defined, implying that there is some interdiffusion between the Cu nanoclusters and the surrounding diamond lattices. On the basis of TEM investigations for the $UNCD_{CuA}$ film, it is noticed that Cu ion implantation/annealing processes induced the formation of nanographitic phases, in concurrence with the Raman and the XPS investigations.

In our previous studies, it has been observed that the existence of grain boundary phases, *a-C* or graphite, surrounding the nano-sized diamond grains of the UNCD films are the prime factors for the enrichment in electrical conductivity and EFE properties of UNCD films.[8,13] Similar conduction mechanism has been applied for explaining the improved electrical conductivity of $UNCD_{CuA}$ films: viz., the Cu ion implantation constructively formed the Cu nanoclusters in the UNCD films and the subsequent annealing process induced the nanographitic phases in the periphery of Cu nanoclusters. The electrons can transported easily through the nanographitic phases to the emitting surface and are then emitted to vacuum without any difficulty as the diamond surfaces are NEA in nature.[5,6] Consequently, the formations of Cu nanoclusters due to Cu ion implantation and the existence of nanographitic phases due to annealing are the genuine factors for the superior EFE properties of the $UNCD_{CuA}$ films.

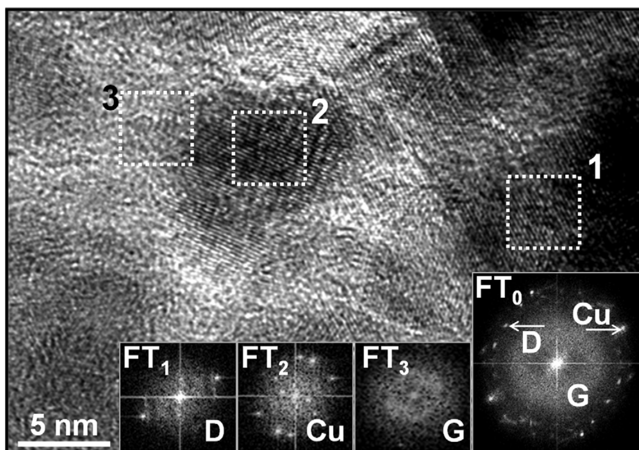

FIG. 8. High resolution TEM structure image corresponding to region A in Fig. 7(a). The FT image corresponding to whole structure image is shown as FT_0 and the FT images of the selected regions marked as 1–3 are shown as insets FT_1–FT_3 images, respectively.

IV. CONCLUSION

In summary, we have demonstrated a feasible way of fabricating conducting UNCD films with enhanced EFE properties due to Cu ion implantation/annealing processes. The $UNCD_{CuA}$ films are highly conducting and show more emission sites in the CITS measurements as compared to $UNCD_P$ films. Presumably, the formations of Cu nanoclusters due to Cu ion implantation and the induction of nanographitic phases among the Cu nanoclusters due to annealing at 600 °C improve the conducting nature of the films that are possibly the major reasons for the enhanced EFE properties of the $UNCD_{CuA}$ films. The superior EFE characteristics of highly conducting UNCD films via simple and robust Cu ion implanted/annealed processes open the prospects of high definition flat panel displays or microplasma based devices.

ACKNOWLEDGMENTS

The authors like to thank the financial support of National Science Council, Taiwan through the Project Nos. NSC 102-2112-M032-006-MY3 and NSC 101-2221-E-007-064-MY3.

[1] W. A. de Heer, A. Chatelain, and D. Ugarte, Science **270**, 1179 (1995).
[2] K. Okano, K. Hoshina, M. Iida, S. Koizumi, and T. Inuzuka, Appl. Phys. Lett. **64**, 2742 (1994).
[3] G. A. J. Amaratunga and S. R. P. Silva, Appl. Phys. Lett. **68**, 2529 (1996).
[4] M. W. Geis, N. N. Efremow, K. E. Krohn, J. C. Twichell, T. M. Lyszczarz, R. Kalish, J. A. Greer, and M. D. Tabat, Nature **393**, 431 (1998).
[5] H. Yamaguchi, T. Masuzawa, S. Nozue, Y. Kudo, I. Saito, J. Koe, M. Kudo, T. Yamada, Y. Takakuwa, and K. Okano, Phys. Rev. B **80**, 165321 (2009).
[6] M. W. Geis, S. Deneault, K. E. Krohn, M. Marchant, T. M. Lyszczarz, and D. L. Cooke, Appl. Phys. Lett. **87**, 192115 (2005).

[This article is copyrighted as indicated in the article. Reuse of AIP content is subject to the terms at: http://scitation.aip.org/termsconditions. Downloaded to] IP: 163.13.36.187 On: Mon, 27 Oct 2014 02:56:23

[7]T. D. Corrigan, D. M. Gruen, A. R. Krauss, P. Zapol, and R. P. H. Chang, Diamond Relat. Mater. **11**, 43 (2002).
[8]K. J. Sankaran, H. C. Chen, C. Y. Lee, N. H. Tai, and I. N. Lin, Appl. Phys. Lett. **101**, 241604 (2012).
[9]J. Birrell, J. A. Carlisle, O. Auciello, D. M. Gruen, and J. M. Gibson, Appl. Phys. Lett. **81**, 2235 (2002).
[10]D. Zhou, A. R. Krauss, L. C. Qin, T. G. McCauley, D. M. Gruen, T. D. Corrigan, R. P. H. Chan, and H. Gnaser, J. Appl. Phys. **82**, 4546 (1997).
[11]J. Birrell, J. E. Gerbi, O. Auciello, J. M. Gibson, D. M. Gruen, and J. A. Carlisle, J. Appl. Phys. **93**, 5606 (2003).
[12]K. J. Sankaran, Y. F. Lin, W. B. Jian, H. C. Chen, K. Panda, B. Sundaravel, C. L. Dong, N. H. Tai, and I. N. Lin, ACS. Appl. Mater. Interfaces **5**, 1294 (2013).
[13]K. J. Sankaran, J. Kurian, H. C. Chen, C. L. Dong, C. Y. Lee, N. H. Tai, and I. N. Lin, J. Phys. D: Appl. Phys. **45**, 365303 (2012).
[14]S. Bhattacharyya, O. Auciello, J. Birrell, J. A. Carlisle, L. A. Curtiss, A. N. Goyette, D. M. Gruen, A. R. Krauss, J. Schlueter, A. Sumant, and P. Zapol, Appl. Phys. Lett. **79**, 1441 (2001).
[15]Y. C. Lin, K. J. Sankaran, Y. C. Chen, C. Y. Lee, H. C. Chen, I. N. Lin, and N. H. Tai, Diamond Relat. Mater. **20**, 191 (2011).
[16]R. Kalish, Carbon **37**, 781 (1999).
[17]S. Talapatra, J. Y. Cheng, N. Chakrapani, S. Trasobares, A. Cao, R. Vajtai, M. B. Huang, and P. M. Ajayan, Nanotechnology **17**, 305 (2006).
[18]S. Prawer and R. Kalish, Phys. Rev. B **51**, 15711 (1995).
[19]K. J. Sankaran, H. C. Chen, C. Y. Lee, N. H. Tai, and I. N. Lin, Appl. Phys. Lett. **102**, 061604 (2013).
[20]X. J. Hu, J. S. Ye, H. J. Liu, Y. G. Shen, X. H. Chen, and H. Hu, J. Appl. Phys. **109**, 053524 (2011).
[21]X. J. Hu, J. S. Ye, H. Hu, X. H. Chen, and Y. G. Shen, Appl. Phys. Lett. **99**, 131902 (2011).
[22]S. M. Sze, *Physics of Semiconductor Devices* (John Wiley & Sons, 1969).
[23]I. Platzman, R. Brener, H. Haick, and R. Tannenbaum, J. Phys. Chem. C **112**, 1101 (2008).
[24]J. Iijima, J. W. Lim, S. H. Hong, S. Suzuki, K. Mimura, and M. Isshiki, Appl. Surf. Sci. **253**, 2825 (2006).
[25]A. L. Stepanov, M. F. Galyautdinov, A. B. Evlyukhin, V. I. Nuzhdin, V. F. Valeev, Y. N. Osin, E. A. Evlyukhin, R. Kiyan, T. S. Kavetskyy, and B. N. Chichkov, Appl. Phys. A **111**, 261 (2013).
[26]J. H. Lee, I. H. Choi, S. Shin, S. Lee, J. Lee, C. Whang, S. C. Lee, K. R. Lee, J. H. Baek, K. H. Chae, and J. Song, Appl. Phys. Lett. **90**, 032504 (2007).
[27]L. Sun, F. Yan, H. Zhang, J. Wang, Y. Zeng, G. Wang, and J. Li, J. Appl. Phys. **106**, 113921 (2009).
[28]V. N. Popok, Rev. Adv. Mater. Sci. **30**, 1 (2012).
[29]V. Resta, L. Calcagnile, G. Quarta, L. Maruccio, A. Cola, I. Farella, G. Giancane, and L. Valli, Nucl. Instrum. Methods Phys. Res. B **312**, 42 (2013).
[30]L. Jiang, T. Yang, F. Liu, J. Dong, Z. Yao, C. Shen, S. Deng, N. Xu, Y. Liu, and H. J. Gao, Adv. Mater. **25**, 250 (2013).
[31]R. H. Fowler and L. Nordheim, Proc. R. Soc. London, Ser. A **119**, 173 (1928).
[32]Z. Sun, J. R. Shi, B. K. Tay, and S. P. Lau, Diamond Relat. Mater. **9**, 1979 (2000).
[33]A. C. Ferrari and J. Robertson, Phys. Rev. B **63**, 121405 (2001).
[34]J. Michler, Y. Von Kaenel, J. Stiegler, and E. Blank, J. Appl. Phys. **83**(1), 187 (1998).
[35]A. C. Ferrari and J. Robertson, Phys. Rev. B **61**, 14095 (2000).
[36]A. Ilie, A. C. Ferrari, T. Yagi, S. E. Rodil, J. Robertson, E. Barborini, and P. Milani, J. Appl. Phys. **90**, 2024 (2001).
[37]Y. F. Chen, Surf. Sci. **380**, 199 (1997).
[38]R. Arenal, P. Bruno, D. J. Miller, M. Bleuel, J. Lal, and D. M. Gruen, Phys. Rev. B **75**, 195431 (2007).
[39]D. M. Gruen, S. Liu, A. R. Krauss, J. Luo, and X. Pan, Appl. Phys. Lett. **64**(12), 1502 (1994).
[40]P. Kovarik, E. B. D. Bourdon, and R. H. Prince, Phys. Rev. B **48**, 12123 (1993).

[This article is copyrighted as indicated in the article. Reuse of AIP content is subject to the terms at: http://scitation.aip.org/termsconditions. Downloaded to] IP: 163.13.36.187 On: Mon, 27 Oct 2014 02:56:23